Astron. Astrophys. 336, 654–661 (1998)

ASTRONOMY AND ASTROPHYSICS

Irregular variables of type Lb

Circumstellar CO emission of an oxygen-rich sample⋆

F. Kerschbaum[1,2] **and H. Olofsson**[2]

[1] Institut für Astronomie, Türkenschanzstrasse 17, A-1180 Wien, Austria
[2] Stockholms Observatorium, S-13336 Saltsjöbaden, Sweden

Received 4 March 1998 / Accepted 11 May 1998

Abstract. We report on the first systematic study of the mass-loss properties of O-rich irregular variables of type Lb. ^{12}CO (*J*=1–0, 2–1, and 3–2) line observations were carried out using the SEST, the Onsala 20 m TELESCOPE, the JCMT and the IRAM 30 m ANTENNA. In total 20 stars were detected among the 31 objects observed (all are new detections; in three cases detections are precluded because of strong interference from interstellar CO emission). Hence, the detection rate is very high for this sample selected on the basis of the 60 μm flux strength. The majority of the detected objects are weak in CO, and the inferred mass-loss rates are low ($\lesssim 10^{-7}\,\mathrm{M}_\odot/\mathrm{yr}$). They have, with only a few exceptions, envelopes with small gas expansion velocities (the mean value is ≈8 km/s). We find that their mass-loss properties are very similar to those of bright O–rich semiregular (SRa or SRb) and Mira variables, i.e., at least in this mass-loss rate range the stellar mass-loss properties are not strongly influenced by the pulsational behaviour of the star.

Key words: stars: variables – stars: AGB – stars: circumstellar matter – stars: mass-loss – radio lines: stars

1. Introduction

The semiregular (types SRa and SRb) and the cool irregular variables (Lb) – quite numerous groups of objects among the stars on the Asymptotic Giant Branch (AGB) – have been almost neglected although their role within the evolution on the AGB and their overall properties are far from being understood. They can provide important constraints for theoretical models due to their different pulsational behaviour compared to the more frequently studied Mira variables. Fortunately, this situation has changed during the last years – at least in the case of the semiregular variables (SRVs). In Kerschbaum & Hron (1992, 1994, 1995; hereafter SR_I, SR_IIa, and SR_III, respectively) and Kerschbaum (1995; hereafter SR_IIb) stellar properties of SRVs, derived from the GCVS4 (Kholopov et al. 1985–88), the IRAS-PSC (1988), the IRAS-LRS (1986), as well as new near infrared photometry, were used to divide this inhomogeneous group of objects into physically distinct classes and to probe their evolutionary status. One of the main outcomes was the definition of O-rich subclasses namley 'blue'-, 'red'-, and 'Mira'-SRVs with the first having short periods (typically below 100 days) and showing no mass-loss. The border between 'red'- and 'Mira'-SRVs is mainly defined by the period (P$<200^d$ for 'red', and P$>200^d$ for 'Mira'). The 'blue'-SRVs seem to be on the early and the other two groups on the thermally pulsing AGB. A study by Jura & Kleinmann (1992) came to similar conclusions concerning the galactic distribution of these stars.

Complementary work on the cool irregular variables of type Lb (IRVs) have to be done in an analogous way, but a major problem is that the IRVs may also act as a kind of "trash group" for poorly observed late-type variables as is partly the case for the SRVs (see Lebzelter et al. 1995). From what is known about the luminosities of IRVs, and since this group contains also Carbon-stars, a significant number of them should be on the thermally-pulsing AGB (Querci 1986). However, Little et al. (1987) found no Technetium, which would be an evidence for a recent thermal pulse, in the O-rich IRVs of their sample.

Peters (1991) used data from the IRAS-mission for an analysis of the space distribution and the mass-loss of the main three AGB-variables: the Miras, the SRVs and the IRVs. The main outcome concerning the latter is that they seem to have mass-loss rates comparable to those of SRVs but smaller than those of Miras. He arrived at similar scale heights for all three groups except for the long-period Miras which were more concentrated to the disk. In a study mainly devoted to SRVs, Jura & Kleinmann (1992) derived a galactic distribution of the IRVs comparable to that of "thin disk" Miras. Unfortunately, their sample was a mixture of IRVs and a significant number of SRVs and Miras with unknown periods. Moreover, it was limited to objects with $|b| \geq 30°$ having GCVS and IRAS-data. All these restrictions did not allow a more detailed analysis.

Recently, Kerschbaum et al. (1996b, hereafter Lb_I) found that their sample of visually bright IRVs displays infrared prop-

Send offprint requests to: F. Kerschbaum,
Internet: kerschbaum@astro.univie.ac.at

⋆ Based on observations collected at the European Southern Observatory, La Silla, Chile, the Onsala Space Observatory, Chalmers Tekniska Högskola, Sweden, the James Clerk Maxwell Telescope, Hawaii and the IRAM 30 m telescope, Pico Veleta, Spain.

erties very similar to the SRVs. As judged from NIR two-colour diagrams the O-rich IRVs seem to have intermediate atmospheric conditions between Miras and normal giants. There may be a slightly larger "contamination" with non-AGB giants than in the case of the SRVs but the AGB objects seem to resemble the 'blue' and the 'red' SRV groups. We note that using only IR-colours the S- and the Carbon-stars among the Lbs are indistinguishable from SRVs of the same chemistry. In the paper by Kerschbaum et al. (1996a), dealing with NIR- and IRAS-photometry, spectral energy distributions, mass-loss rates from IRAS-data, galactic distribution and the evolutionary status of O-rich AGB-variables, the similarity between the IRVs and SRVs was demonstrated in many more aspects.

Besides the dust mass-loss derived from IRAS photometry circumstellar CO emission has proven to be a good measure of the gas mass-loss rate. Whereas quite a lot has been done for evolved AGB objects like Carbon-stars (Kastner et al. 1993; Nyman et al. 1992; Olofsson et al. 1993; Groenewegen et al. 1996), OH/IR-stars (Heske et al. 1990), and more recently S-stars (Bieging & Latter 1994; Sahai & Liechti 1995; Groenewegen & de Jong 1998), the low end of the mass-loss rate distribution, populated by objects situated on the early AGB, or at the beginning of the thermally pulsing AGB, has not been studied in any detail.

Kahane & Jura (1994) published high quality observations of 11 nearby O-rich SRVs in the CO (J=1–0 and 2–1) lines. They came to the conclusion that these short-period objects have mass-loss properties quite similar to those of longer-period Miras. Kerschbaum et al. (1996c, hereafter SR_IV) extended this work considerably in their study of O-rich SRVs. The majority of their detected objects, covering both small and longer periods, are weak in CO, i.e., they are low mass-loss rate objects ($\lesssim 10^{-7}\,\mathrm{M}_\odot/\mathrm{yr}$), and have in general envelopes with small expansion velocities (the mean value is ≈8 km/s).

A recent CO (J=3–2) study was devoted to nearby, optically bright O-rich Miras (Young 1995, Y95), whose periods are 2–3 times higher than those of the SRVs (they are probably pulsating in a lower pulsational mode). Among the results we note that the average circumstellar gas expansion velocity of this volume-limited sample is small compared to that of bright infrared Miras (see e.g., Nyman et al. 1992) and Carbon-stars (Olofsson et al. 1993), and that the mass-loss rates are low and increase with decreasing effective temperature.

These studies suggest that the mass-loss properties of the bright O-rich SRVs and Miras are very similar and hence support the view that the mass-loss is not strongly affected by the pulsational mode, at least not in this mass-loss rate regime ($\lesssim$ few $\times\, 10^{-7}\,\mathrm{M}_\odot/\mathrm{yr}$).

2. Observations

2.1. The sample

Well studied O-rich IRVs were selected on the basis of their IRAS-60 μm fluxes in order to detect them in circumstellar CO emission for the first time. Based on our experience with the SRVs (SR_IV) only objects redder than –1.2 in the IRAS-colour [12]–[25] were observed in order to save observing time. This biased our sample towards mass losing objects of similar properties like 'red' and 'Mira'-SRVs. The names in the GCVS4 and the IRAS-PSC of the 31 observed stars are given in Table 1. The source coordinates were taken either from the Hipparcos Input Catalogue (Turon et al. 1994) or from SIMBAD where most of the objects have coordinates of subarcsecond accuracy.

2.2. Observational results

The observations in the CO (J=1–0) line were performed with the Swedish-ESO Submillimetre Telescope (SEST), La Silla, Chile, and the 20 m telescope at Onsala Space Observatory (OSO), Sweden. CO (J=2–1) line data come from SEST, the IRAM 30 m telescope, Pico de Veleta, Spain, and the James Clerk Maxwell Telescope (JCMT), Mauna Kea, Hawaii, while the CO (J=3–2) line was observed only with the JCMT. Table 1 summarizes the results. In total 20 stars were detected (all are new detections). In three cases detections are precluded because of strong interference from interstellar CO emission. In total there are 43 individual measurements because some stars were observed in more than one line. The first letter of the code gives the observatory (**I**RAM, **J**CMT, **O**SO, or **S**EST), the rest the transition observed. Another code reflects the "success" of detection (**D**etection, or **N**on-detection). An 'i' indicates contamination by interstellar CO lines. More detailed information about the observations and all the individual spectra are found in Kerschbaum & Olofsson (in preparation).

When determening the line parameters we compared the results of fitting parabolas or 4^{th} order polynomials, which generally fit the lines very well, with eye estimates of where the profiles go to zero intensity. Both approaches agreed well in most of the cases. We determined the zero intensity velocities (i.e., the velocities at the two edges of the line profile) from the best fits. The stellar velocity was then derived from the average of these velocities, and the gas expansion velocity of the envelope from half the difference between these velocities. Before doing this we removed the major baseline irregularities by fitting low order polynomials to the spectra. We estimate that both quantities are uncertain by about 1–2 km/s, but the uncertainty varies with the S/N-ratio. This means that the low expansion velocities may be uncertain by up to 30%, while for the highest expansion velocities the uncertainty decreases to about 10%. The stellar velocity is given with respect to the heliocentric (v_{hel}) and the LSR frame [v_{LSR}; the Local Standard of Rest is defined using standard solar motion (B1950.0): $v_\odot = 20\,\mathrm{km/s}$, $\alpha_\odot = 270\overset{\circ}{.}5$, $\delta_\odot = +30\overset{\circ}{.}0$]. The peak main beam brightness temperature, T_{mb}, is obtained as an average of the line profile intensities in the velocity range $v_{\mathrm{hel}} \pm 0.2 v_{\mathrm{exp}}$. The integrated intensity, $I = \int T_{\mathrm{mb}} dv$, is obtained by integrating the line intensities over the velocity range $v_{\mathrm{hel}} \pm v_{\mathrm{exp}}$. Once again the uncertainty in both quantities varies with the S/N-ratio, but we estimate that it is on average about 20%, and in the worst cases it may reach 50%. To this should be added an estimated uncertainty in the absolute calibration of about 20%. In no case do

Table 1. Observational results of O-rich Lb variables

GCVS4	IRAS	Code	S	I (Kkm/s)	$T_{\rm mb}$ (K)	$v_{\rm hel}$ (km/s)	$v_{\rm LSR}$ (km/s)	$v_{\rm exp}$ (km/s)	Q
CE And	01265+4624	O10	N	0.72					5
		J32	D	1.71:	0.10	–17.5	–14.6:	11.5:	4
EX Ori	05220−0611	S21	D	0.52	0.07	–12.6	–30.6	5.2	2
		J32	D	2.30	0.18	–12.7	–30.8:	8.0:	4
V352 Ori	05592−0221	S21	Di	0.38	0.04	38.8	21.1:	8.4:	2
DW Gem	06278+2729	O10	N	0.31					5
FZ Hya	08189+0507	O10	N	0.71					5
		S21	D	1.67	0.12	0.5	–12.9	10.4	2
		J32	D	4.56	0.35	0.1	–13.3	8.3	1
OT Pup	08200−2528	S21	D	1.48	0.10	48.1	30.9	10.6	1
		J32	D	6.82	0.39	48.0	30.8	13.6	2
FK Hya	08220−0821	S21	D	0.37	0.02	55.5	40.0	12.6	3
		J32	N	0.63					5
CW Cnc	09057+1325	O10	D	2.51	0.16	26.7	17.3	8.4	2
		S21	D	4.29	0.25	25.3	15.9	9.9	1
		J32	D	14.61	1.01	25.0	15.6	10.5	1
CT UMa	10305+7001	O10	N	0.65					5
CS Dra	11125+7524	O10	D	1.34	0.06	–58.5	–49.8	11.6	3
		J32	D	3.84	0.29	–59.1	–50.3	8.8:	3
AZ UMa	11445+4344	O10	D	0.58	0.08	–49.7	–43.7	4.0	3
		J32	D	4.42	0.62	–49.5	–43.5	5.5	1
RW Vir	12046−0629	S21	D	1.88	0.17	21.8	20.9	8.0	1
		J32	D	6.88	0.56	22.3	21.3	7.2	1
TY Dra	17361+5746	O10	D	1.08	0.06	–34.9	–17.3:	9.7:	2
TU Lyr	18186+3143	O10	N	0.73					5
CZ Ser	18347−0241	I10	Di	3.85:	0.21	–31.1	–14.5:	9.2:	3
		I21	Di	11.43	0.71	–31.5	–14.8	9.8	2
YZ Lyr	19014+2904	O10	N	0.80					5
SZ Dra	19098+6601	O10	D	0.77	0.05	–42.0	–26.1:	9.6:	3
V1943 Sgr	20038−2722	J32	D	34.48:	3.45	–23.7	–15.0	6.5	2
V584 Aql	20079−0146	S21	D	0.87	0.12	–13.6	0.9	3.3	2
Y Tel	20165−5051	S21	D	0.77	0.10	–45.8	–44.5:	5.9:	3
TZ Aql	20276−0455	S21	D	0.62	0.07	49.1	62.1	6.2	2
V397 Cyg	20302+3517	O10	Ni	1.62					5
FI Vul	20466+2248	O10	N	1.14					5
IN Vul	20511+2523	O10	N	2.79					5
AB Aqr	22359−1417	S21	D	0.85	0.10	29.3	33.1	5.1	2
BC And	22586+4614	O10	D	0.58	0.08	–12.2	–1.7:	4.5:	3
V352 Cep	22594+6117	O10	Ni						5
AS Cep	23000+5932	O10	N	1.35					5
CF And	23013+3735	O10	N	0.44					5
SV Aqr	23201−1105	S21	D	1.23	0.09	4.7	5.9	7.9	2
V530 Cas	23284+5958	O10	Ni						5

we expect that these uncertainties in the line profile characteristics will have any significant effect on the conclusions drawn in this paper. For a non-detection an upper limit to I is estimated by measuring the peak-to-peak noise ($T_{\rm pp}$) of the spectra with a velocity resolution reduced to 15 km/s and calculating $I = 15T_{\rm pp}$. The last column of Table 1 gives a quality ranking ranging from 5 (useless, nondetection) to 1 (very good). A spectrum must have quality 3 or better to be used in the analysis. Similar visual inspection was carried out also for the literature data that we used.

Some examples of spectra are shown in Fig. 1. The velocity scale is given in the heliocentric system. Within the limitations of the S/N-ratio all of the line profiles in our sample lie in the range of the expected, i.e., between a rectangular (spatially unresolved, optically thin emission) and a parabolic (spatially unresolved, optically thick emission) line shape.

3. Gas expansion velocities

We will compare stellar and circumstellar characteristics of the IRVs, SRVs, and Miras in this and the next section. For a com-

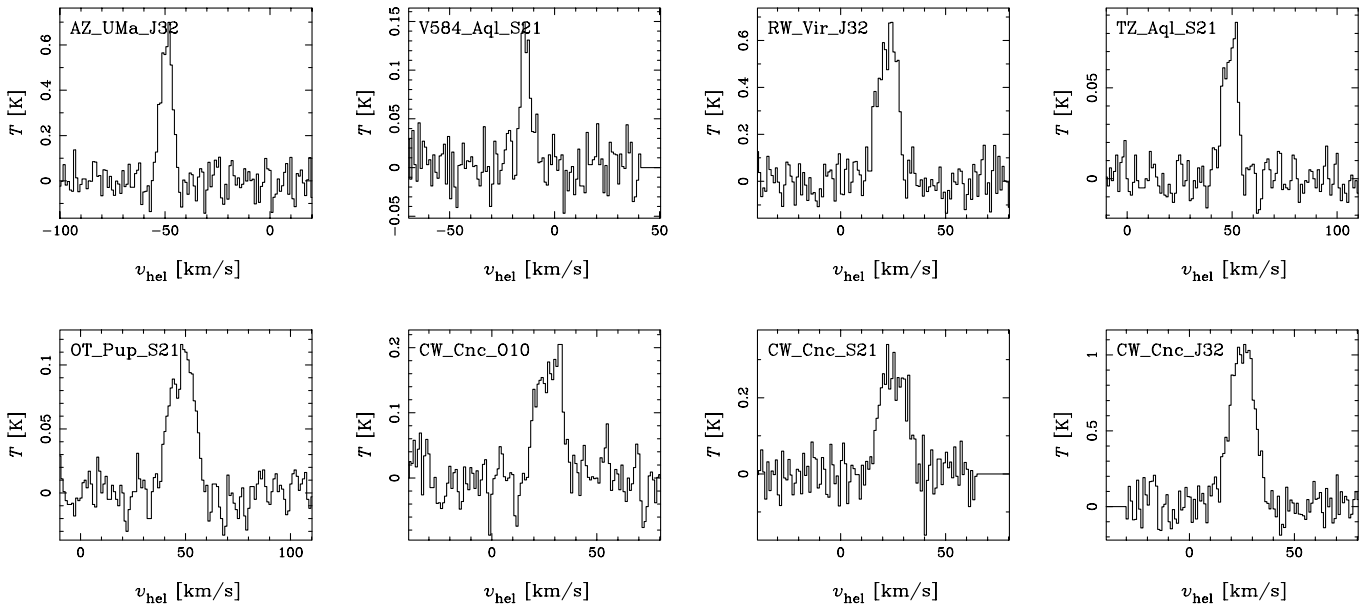

Fig. 1. Examples of CO spectra of O-rich Lb variables. The intensity scale is in main beam brightness temperature

parison with SRVs and Miras additional data from the literature were used (Young 1995, Loup et al. 1993, Kahane & Jura 1994, SR_IV), as well as new observations of SRVs presented in a catalogue paper (Kerschbaum & Olofsson in preparation). According to the classification scheme for SRVs presented in Kerschbaum & Hron (1992) the SRVs are split into 'blue'-, 'red'-, and 'Mira'-SRVs with the first ones being ignored here since they show no mass-loss. For the plots the border between 'red'- and 'Mira'-SRVs is defined by period (P$<200^d$ for 'red', and P$>200^d$ for 'Mira').

3.1. Distribution

Whereas mass-loss rates taken from the literature often differ substantially, expansion velocities can easily be derived without too many assumptions even from lower S/N-ratio spectra. Consequently, using $v_{\rm exp}$ larger comparison samples are available. If for an individual object more than one independent measurement of $v_{\rm exp}$ are available the best was chosen, or, if they are of comparable quality, they were averaged.

The majority of the detected IRVs and SRVs have, with few exceptions, envelopes with small expansion velocities, Fig. 2. They range from 3 to 15 km/s with a mean value around 8 km/s for both groups. Except for a few objects with expansion velocities above 15 km/s the Miras cover the same velocity range and have roughly the same distribution. In particular, all three groups of variables show a number of very low expansion velocity objects (below 6 km/s) like the IRVs V584 Aql and AZ UMa shown in Fig. 1.

The measured expansion velocities are comparable to the terminal velocities derived by Netzer & Elitzur (1993) in models of O-rich objects with mass-loss rates between a few 10^{-7} to 10^{-6} $\mathrm{M}_\odot$/yr.

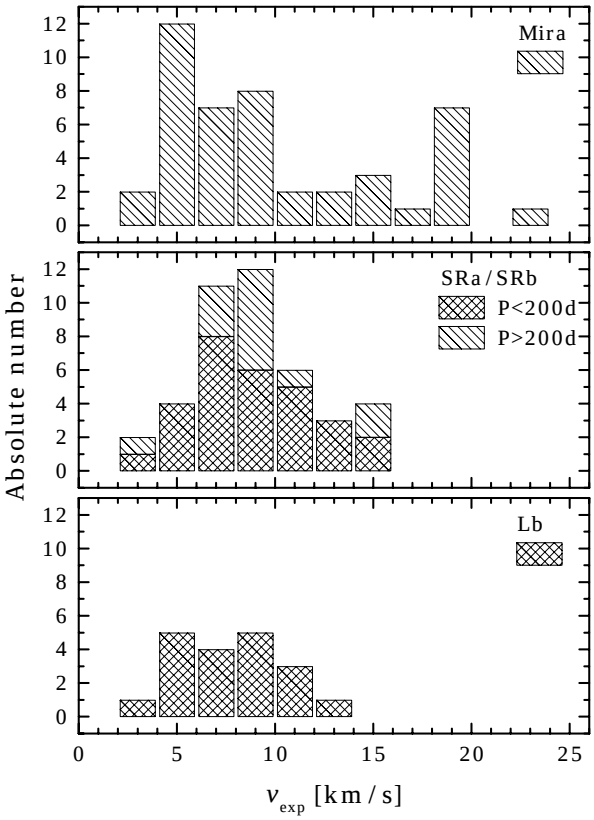

Fig. 2. Distribution of expansion velocities

3.2. Stellar parameters

3.2.1. Visual amplitude

In Fig. 3 we have plotted the gas expansion velocity as a function of the V-amplitude listed in the new Tycho-Catalogue (ESA

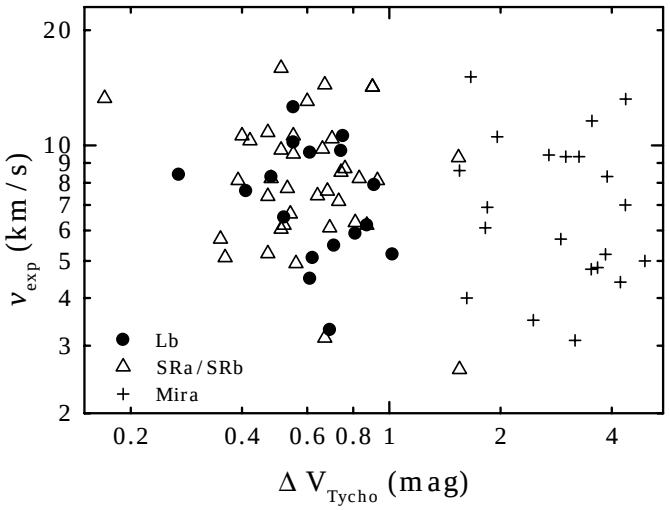

Fig. 3. Expansion velocity as a function of Tycho-amplitude

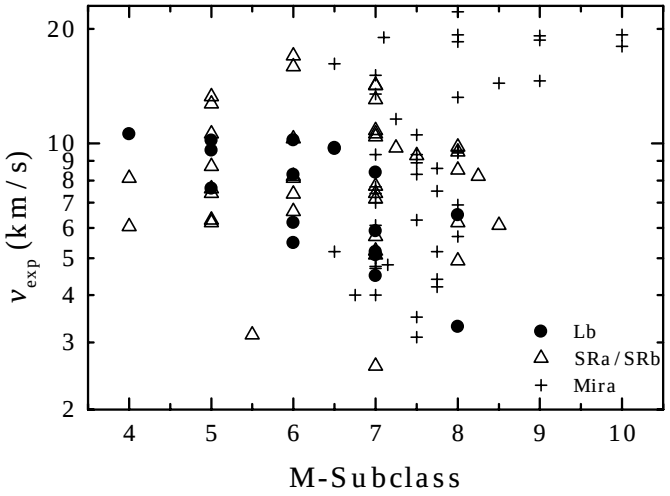

Fig. 4. Expansion velocity as a function of mean M-subclass

1997). For all three groups of variables there appears to be no trend in expansion velocity with amplitude. The distributions of the IRVs and the 'red'-SRVs are indistinguishable from each other and well separated from that of the 'Mira'-SRVs and the Miras.

3.2.2. M-subclass

The comparison with the averaged M-subclass (GCVS4), which mainly reflects the stellar effective temperature, shows some trends, Fig. 4. The lowest expansion velocities are found between M6.5 and M8 (but this could be an effect of the larger number of stars in this range). The intermediate expansion velocities (6–12 km/s) are found for a wide range of spectral classes (M4–M8), with the 'hotter' stars being mainly IRVs and 'red'-SRVs. High expansion velocities are only found for late-type Miras.

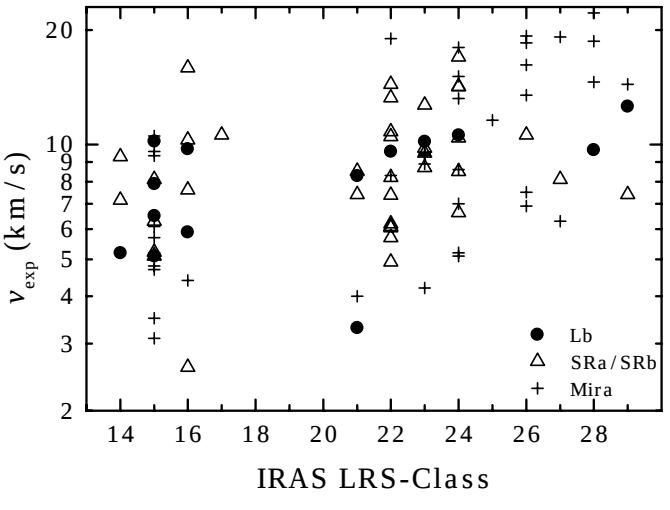

Fig. 5. Expansion velocity as a function of IRAS LRS-class

3.2.3. IRAS LRS-class

An independent quantity measuring dust mass-loss is the IRAS LRS-class. In Fig. 5 we plot $v_{\rm exp}$ versus the IRAS LRS-class. A clear trend is visible. The objects with the strongest silicate emission feature (high 2*n* class) show the highest expansion velocities. Low $v_{\rm exp}$ is accompanied by a low 2*n* class. The IRVs and the 'red'-SRVs mostly show only a weak silicate emission feature indicating low mass-loss rates. For all groups of variables also objects without a clear emission feature (only a 'flat' continuum; LRS-classes 14–16) are found, and they have with only one exception expansion velocities below ≈10 km/s. Thus, it appears that the expansion velocity increases with the efficiency of the mass loss process.

4. Gas mass-loss rate deduced from CO data

In accordance with SR_IV we derive gas mass-loss rates using Kastner's (1992) self-consistent model calculations for circumstellar CO emission (in fact, they apply only to C-rich envelopes where CO is the dominant coolant). He solved the energy balance equation for the expanding circumstellar gas simultaneously with the radiative transfer for the CO line emission. One of the results was a formula for estimating the stellar gas mass-loss rate from the CO (J=1–0) antenna temperature, $T_{\rm mb}$ (in K), and the expansion velocity, $v_{\rm exp}$ (in km/s), of an envelope with unresolved emission,

$$\dot{M}_{\rm CO}^{\rm gas} = 8.5 \cdot 10^{-13} \frac{1}{d^2} \left(\frac{T_{\rm mb}}{0.08} \right)^{\alpha} v_{\rm exp}^2 D^2 \frac{10^{-3}}{f_{\rm CO}} \, {\rm M}_{\odot}/{\rm yr} \,, \quad (1)$$

where d (in m) is the diameter of the telescope, D (in pc) is the distance to the source, and $f_{\rm CO}$ is the abundance of CO with respect to H_2. A value of 2×10^{-4} was adopted for the latter (Smith & Lambert 1985). An α of 0.5 was used for our low mass-loss rate sample (see below). We used the same formula for the CO (J=2–1) and CO (J=3–2) data, except that the $T_{\rm mb}$-values were divided by 5 and 15, respectively (see next section for a short discussion of line intensity ratios).

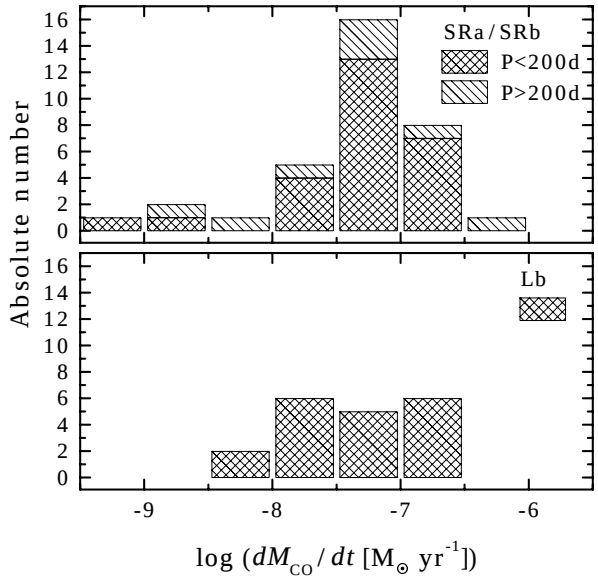

Fig. 6. Distribution of gas mass-loss rates

In order to estimate distances a luminosity L=5000 $L_\odot$ was adopted following the work of Jura & Kleinmann (1992). The $m_{\rm bol}$ values for the individual objects were obtained by integrating the energy distributions ranging from visual data over the near infrared to the IRAS-range. Table 2 lists the estimated distances, D (in pc), for all objects having the information required to derive the bolometric magnitudes. The values are rounded to multiples of 10.

We are aware that Eq. 1 may lead to considerable systematic errors in the mass-loss rate estimates (see e.g., SR_IV), but we believe that it contains the proper dependences of the mass-loss rate on the observed intensity, expansion velocity, and distance. In this way it can be used to reliably study the relative differences in the mass-loss rates within, as well as between, the different variablity groups.

In Table 2 the derived values of $\dot{M}_{\rm CO}^{\rm gas}$ are given for all stars and all transitions. A code gives the origin (as in Table 1) of the CO data and the observed transition (10, 21, 32). Taken at their face values, it is clear that, as expected, all of our sources are low mass-loss rate objects, i.e., $\dot{M}_{\rm CO}^{\rm gas} \lesssim 10^{-7} {\rm M}_\odot/{\rm yr}$. Figure 6 shows the distribution of the gas mass-loss rates of our new IRV-sample in comparison with the SRVs taken from SR_IV and the new material in Kerschbaum & Olofsson (in preparation). It is clear that we are not covering the whole range with our small IRV-sample, but it seems that they populate a similar mass-loss regime to the SRVs.

5. Line intensity ratios

Since we observed more than one transition per star for a few objects mean line intensity ratios can be deduced. An example of multi-line observations is shown in Fig. 1 (CW Cnc).

The combined results (IRVs and SRVs) for the different J levels of ^{12}CO are 5 for I(2–1)/I(1–0), 3 for I(3–2)/I(2–1) and around 1 for I(CO(4–3)/I(3–2). All these ratios differ a lot from star to star. The first two ratios for IRVs alone are between 3 and 4 and within the limitations of our very small sample identical with the values given above. Uncertainties of the absolute calibrations of the different antennas add propably additional scatter.

Nevertheless, it seems clear that we observe a different behaviour than in the case of optically thick Mira variables where a ratio of 2 is typical for I(2–1)/I(1–0). Groenewegen et al. (1995) found for their sample of short period (P<400^d) O-rich Miras these large ratios, too. They argued that the excitation properties in such thin shells are maybe very different and that possibly radiative excitation could be more important that one by collisions. The situation will be clearer with more objects observed in more than one transition. These multiline observations will also play a crucial role for the forseen modelling.

6. Dust mass-loss rate deduced from the IRAS 60 μm flux

The dust mass-loss rate is obtained from the following formula, based on the results of Jura (1987) and adopted in the form given by Olofsson et al. (1993),

$$\dot{M}_{60}^{\rm dust} = 2.6 \cdot 10^{-8} F_{60}^{\rm dust} v_{\rm dust} D^2 \left(\frac{150}{\chi_{60}}\right) \frac{1}{\sqrt{\nu_0 L}} \, {\rm M}_\odot/{\rm yr}, \quad (2)$$

where $F_{60}^{\rm dust}$ is given in Jy, the dust velocity $v_{\rm dust}$ in km/s, D in pc, the luminosity L in $L_\odot$, and a grain emissivity at 60 μm, χ_{60}, of 150 cm^2/g has been adopted. For our low mass-loss rate objects the maximum of the spectral energy distribution ν_0 (in Hz) can be calculated from Wien's law, $\nu_0 = 6 \cdot 10^{10} T_{\rm eff}$, with $T_{\rm eff}$ (in K) taken from blackbody fits, corrected according to SR_III as $T_{\rm eff} = T_{\rm BB}^\star + 500$.

Following the approach of paper SR_IV we corrected for the fraction of the 60μm flux that originates in the stellar photosphere by fitting blackbodies to the broad-band spectra (see SR_III). Corrections of about 10 % were typical within a total range of 5–25 %.

In low mass-loss rate objects the drift velocity between the gas and the dust can be substantial. According to (Kwok 1975) the dust velocity is given by

$$v_{\rm dust} = v_{\rm exp} + \sqrt{\frac{v_{\rm exp} Q L}{c \dot{M}_{\rm g}}}, \quad (3)$$

where Q is the absorption efficiency of the dust grains (assumed to be 1.5×10^{-2} according to Huggins et al. 1988). We assume that Eq. (3) gives a reasonable upper limit to the dust velocity. For the lowest mass-loss rate objects this formula may result in drift velocities exceeding the limit when substantial grain sputtering is expected to occur, i.e., ≈ 20 km/s (Kwok 1975). In a few cases one consequently has to limit the drift velocity to this value, i.e, let $v_{\rm dust} = v_{\rm exp} + 20$. The resulting dust mass loss rate estimates are given in Table 2. The $\dot{M}_{\rm CO}/\dot{M}_{60}^{\rm dust}$ range between 10 and 300, with a median of ≈40. This value is so low that one suspects that either the gas mass loss rate is underestimated or else the dust mass loss rate is overestimated. See Sect. 3.5 of SR_IV for a short discussion of the problem. Detailed modelling

Table 2. Estimated mass-loss rates

GCVS4	IRAS	D (pc)	Code	$v_{\rm exp}$ (km/s)	$\dot{M}_{\rm CO}$ ($M_\odot$/yr)	$\dot{M}_{60}^{\rm dust}$ ($M_\odot$/yr)	$\dot{M}_{\rm CO}/\dot{M}_{60}^{\rm dust}$	Q
EX Ori	05220−0611	570	S21	5.2	1.7E−08	4.1E−10	4.3E+01	2
V352 Ori	05592−0221	320	S21	8.4	1.0E−08	5.6E−10	1.9E+01	2
FZ Hya	08189+0507	450	J32	8.3	1.3E−08	4.5E−10	3.0E+01	1
OT Pup	08200−2528	570	S21	10.6	8.5E−08	4.9E−10	1.7E+02	1
FK Hya	08220−0821	280	S21	12.6	1.4E−08	3.4E−10	4.0E+01	3
CW Cnc	09057+1325	420	S21	9.9	6.4E−08			1
CS Dra	11125+7524	410	O10	11.6	2.3E−07			3
AZ UMa	11445+4344	450	J32	5.5	7.9E−09	5.7E−10	1.4E+01	1
RW Vir	12046−0629	420	S21	8.0	3.6E−08	2.8E−10	1.3E+02	1
TY Dra	17361+5746	480	O10	9.7	2.1E−07	7.3E−10	2.9E+02	2
CZ Ser	18347−0241	570	I21	9.8	5.1E−08	1.2E−09	4.1E+01	2
SZ Dra	19098+6601	590	O10	9.6	2.9E−07			3
V1943 Sgr	20038−2722	210	J32	6.5	5.6E−09	4.8E−10	1.2E+01	2
V584 Aql	20079−0146	500	S21	3.3	7.1E−09	4.8E−10	1.5E+01	2
Y Tel	20165−5051	490	S21	5.9	1.9E−08	4.8E−10	4.0E+01	3
TZ Aql	20276−0455	580	S21	6.2	2.5E−08	5.7E−10	4.4E+01	2
AB Aqr	22359−1417	610	S21	5.1	2.2E−08	4.8E−10	4.7E+01	2
BC And	22586+4614	700	O10	4.5	1.1E−07	1.5E−09	7.4E+01	3
SV Aqr	23201−1105	560	S21	7.9	4.4E−08	4.7E−10	9.2E+01	2

of both dust and gas mass-loss will be needed to arrive at final results.

In our sample it turns out that a typical $v_{\rm dust}$ is around 16 km/s. We used this value for large samples of visual O-rich Miras, SRVs and Lbs in order not to be limited to the small number of objects were $v_{\rm dust}$ can be derived from an observed $v_{\rm exp}$.

Figure 7 shows the resulting distributions in dust mass-loss rates derived in the way described above. The result is comparable to that from the CO observations thus indicating that our small CO sample was not affected by too strong biases. A relatively small range of mass-loss rates is found for all three groups. This further emphasizes that the mass-loss properties appear not to be strongly influenced by the pulsational regularity or even the mode.

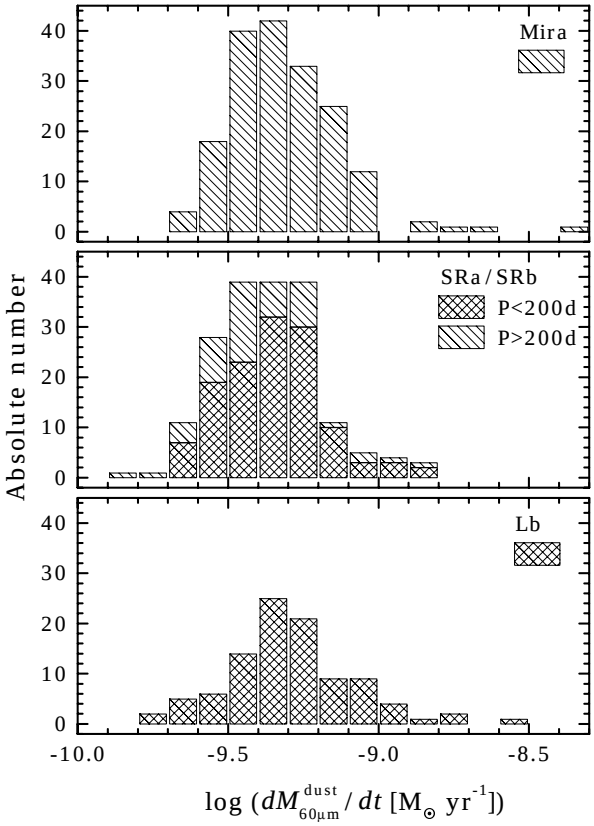

Fig. 7. Distribution of dust mass-loss rates

7. Conclusion and outlook

We have for the first time detected a larger sample of O-rich irregularly variable red giants (variability type Lb) in circumstellar CO emission, a signpost of circumstellar envelopes produced by stellar mass-loss. The majority of the detected objects are weak in CO, and the estimated mass-loss rates are low, $\lesssim 10^{-7}\,M_\odot$/yr. The envelope gas expansion velocities are, with only a few exceptions, small (the mean value is ≈8 km/s, but we find objects with velocities as low as ≈3 km/s!).

A comparison between stellar and circumstellar properties of these stars and samples of O-rich SRVs and Miras shows that, at least in the mass-loss rate range studied here, the gas expansion velocity does not depend on the stellar effective temperature, nor on the pulsational amplitude or period of the star. Likewise, the mass-loss rate distributions are very similar for these three groups of variables. Consequently, the stellar mass-loss properties seem not to be strongly influenced by the pulsational regularity or even the mode (compare SR_III and SR_IV).

There is a trend of increasing gas expansion velocity with the IRAS LRS-class (2n), which suggests that the expansion velocity increases along with the mass loss rate.

For the future we propose observations of higher-J lines of CO (since the line intensity increases substantially with frequency) as well as other molecules in order to determine the physical and chemical characteristics of these relatively warm envelopes. In general, this type of envelopes are not so well studied, and in a forthcoming paper we will analyze the CO and the dust emission from the envelopes of IRVs and SRVs in much more detail. The most nearby objects can be mapped in suitable molecular emissions with mm-wave interferometers. This is of special importance for these low mass-loss rate objects where the higher frequency of peculiar line profiles suggest a complex envelope structure. In order to investigate the dust mass loss properties of IRVs a small number of typical objects are observed with the Short Wave Spectrometer on board the ISO satellite.

Acknowledgements. The work of FK was supported by APART (Austrian Programme for Advanced Research and Technology) from the Austrian Academy of Sciences. FK was also supported by the Fonds zur Förderung der wissenschaftlichen Forschung under project number S7308-AST and the Österreichische Nationalbank under the Jubiläumsfonds-project number 6876. HO acknowledges financial support from the Swedish Natural Science Research Council.

The authors are very grateful to Göran Sandell for carefully performing the JCMT observations, and thank Martin Groenewegen for providing us with the IRAM spectra of CZ Ser. The reduction of the CO spectra was made using the DRP software kindly provided by Michael Olberg, OSO.

The Swedish-ESO Submillimetre Telescope, SEST, is operated jointly by ESO and the Swedish National Facility for Radio Astronomy, Onsala Space Observatory at Chalmers University of Technology. The James Clerk Maxwell Telescope is operated by The Joint Astronomy Centre on behalf of the Particle Physics and Astronomy Research Council of the United Kingdom, the Netherlands Organisation for Scientific Research, and the National Research Council of Canada. This research has made use of the SIMBAD database.

References

Bieging J.H., Latter W.B. 1994, ApJ 422, 765
ESA 1997, The Hipparcos and Tycho Catalogues, ESA SP-1200
Groenewegen M.A.T., Baas F., Blommaert J., Josselin E., Tilanus R.P.J. 1995, in: "Science with large millimetre arrays", Dec. 1995, Garching, Ed. P. Shaver, Springer Verlag, p. 286
Groenewegen M.A.T., Baas F., de Jong T., Loup C. 1996, A&A 306, 241
Groenewegen M.A.T., de Jong T. 1998, A&A (in press)
Heske A., Habing H.J., Forveille T., Omont A., van der Veen W.E.C.J. 1990, A&A 239, 173
Huggins P.J., Olofsson H., Johansson L.E.B. 1988, ApJ 332, 1009
IRAS Science Team 1986, A&ASS 65, 607 (IRAS-LRS)
IRAS Science Team 1988, IRAS Catalogs and Atlases, Volumes 2–6, NASA RP–1190 (IRAS-PSC)
Jura M. 1987, ApJ 313, 743
Jura M., Kleinmann S.G. 1992, ApJS 79, 105
Kahane C., Jura M. 1994, A&A 290, 183
Kastner J.H. 1992, ApJ 401, 337
Kastner J.H., Forveille T., Zuckerman B., Omont A. 1993, A&A 275, 163
Kerschbaum F., Hron J. 1992, A&A 263, 97 (SR_I)
Kerschbaum F., Hron J. 1994, A&AS 106, 397 (SR_IIa)
Kerschbaum F. 1995, A&AS 113, 441 (SR_IIb)
Kerschbaum F., Hron J. 1996, A&A 308, 489 (SR_III)
Kerschbaum F., Habison P., Hron J. 1996a, Proc.: The Carbon Star Phenomenon, I.A.U. Symposium 177, Kluwer Academic Publishers, Dordrecht, in press
Kerschbaum F., Lazaro C., Habison P. 1996b, A&AS 118, 397 (Lb_I)
Kerschbaum F., Olofsson H., Hron J. 1996c, A&A 311, 273 (SR_IV)
Kerschbaum F., Olofsson H. 1998, A&AS, in preparation
Kholopov P.N. et al. 1985–88, General Catalogue of Variable Stars, 4^{th} edition, "Nauka" P ublishing House, Moscow (GCVS4)
Lebzelter T., Kerschbaum F., Hron J. 1995, A&A 298, 159
Little S.J., Little-Marenin I.R., Hagen Bauer W. 1987, AJ 94, 981
Loup C., Forveille T., Omont A., Paul J.F. 1993, A&AS 99, 291
Netzer N., Elitzur M. 1993, ApJ 410, 701
Nyman L.-Å., Booth R.S., Carlström U. et al. 1992, A&AS 93, 121
Olofsson H., Eriksson K., Gustafsson B., Carlström U. 1993, ApJS 87, 267
Peters W.J. 1991, Master Thesis, Univ. Amsterdam.
Querci F.R. 1986, In: The M-type stars, eds. H.R. Johnson, F.R. Querci, NASA SP–492, p. 1–113
Sahai R., Liechti S. 1995, A&A 293, 193
Smith V.V., Lambert D.L. 1985, ApJ 294, 326
Turon C. et al. 1992, Hipparcos Input Catalogue, ESA SP-1136
Young K. 1995, ApJ 445, 872 (Y95)